MALAYSIAN JOURNAL OF MICROSCOPY

Journal homepage: https://malaysianjournalofmicroscopy.org

RESEARCH ARTICLE

SYNTHESIS AND CHARACTERISATION OF PHOSPHORUS-DOPED AKERMANITE-BASED BIOCERAMICS

Fitria Pebriani Naibaho, Yanny Marliana Baba Ismail*

School of Materials and Mineral Resources Engineering, Engineering Campus, University Sains Malaysia, 14300 Nibong Tebal, Penang, Malaysia

Abstract. Synthetic akermanite ($Ca_2MgSi_2O_7$) ceramics are viewed as promising candidates for bone implants due to their superior mechanical and bioactive properties compared to CaP-based ceramics. This paper investigates the effect of substituting phosphorus (P^{5+}) ions on the physical, chemical/elemental, and morphological characteristics of akermanite-based powders produced at ambient conditions. To make the composition closer to our native bone, phosphate ions (P^{5+}) were introduced into the akermanite host structure within controlled amounts, $Ca_2MgSi_{2-x}P_xO_7$ (where x = 1, 1.5, 2.5, and 3.5 mol%). The powders were synthesised using planetary ball milling at 400 rpm for 4 hours, and the slurry was heated in the electric oven at 100 °C for 10 hours. X-ray diffraction pattern of the as-milled powders revealed no distinct akermanite phase, likely due to the poor crystallinity of the samples, as the synthesis was conducted at low temperature. However, a slight shift of the broad peaks toward higher angles was observed with increasing P^{5+} substitution, suggesting structural changes in the short-range of the material. No apparent changes were observed in the functional groups detected, as the amount of dopant was relatively small. The elemental analysis confirmed the partial substitution of P^{5+} into the akermanite structure, with the amount of phosphorus increasing with increasing Phosphorus Pentoxide (P_2O_5). Despite the varying compositions, all the powders formed agglomerated particles due to the Van der Waals attractive forces between the particles. Based on physicochemical analyses, the optimum concentration of P^{5+} was found at 3.5 mol%. These findings indicate that P-doped akermanite-based materials provide valuable insights for use in orthopaedic applications.

Keywords: Akermanite, P-doped akermanite, planetary ball milling.

Article Info

Received 10 January 2025
Accepted 27 February 2025
Published 2 June 2025

***Corresponding author: yannymarliana@usm.my**

ISSN: 1823-7010, eISSN: 2600-7444

1. INTRODUCTION

β-tricalcium Phosphate and Hydroxyapatite (HA) are well-known bioceramic materials for orthopaedic applications. However, research has shown that HA has a modest rate of biological activity and a limited capacity to build an interface with tissue. As an alternative to CaP-based materials, calcium silicate ceramics such as akermanite ($Ca_2MgSi_2O_7$) have currently been classified as prospective materials for orthopaedic implants and substituted element within the ceramic-polymeric composite [1, 2]. This akermanite ceramic has been used in comparative studies alongside phosphate-based ceramic materials, such as hydroxyapatite and β-tricalcium phosphate [3, 4].

The production of calcium silicate ceramics may involve wet or dry chemical techniques, including the combustion method [5], the sol-gel method [6], and the mechanical milling method [1]. Ball milling is a mechanical processing approach for solid-state powders that has been utilised to produce nanosized materials due to the advantages of being affordable, easy to control stoichiometry, and simple synthesis method [7]. The milling method is a pivotal step in producing nanopowders in bioceramics.

Akermanite ($Ca_2MgSi_2O_7$) is a promising bone substitute owing to its high strength and controlled degradability compared to HA [8]. It is well known that calcium (Ca) and phosphorus (P) are the primary elements found in the biological apatite, which forms the inorganic component of human bone and also plays a significant role in promoting mineralisation [9]. As akermanite degrades, calcium, magnesium, and silicon ions can be released into tissue. These bioactive ions can enhance bone regeneration and related growth factors [7, 10]. Magnesium (Mg) ions help with osteogenesis, while silicon ions support collagen formation and mineralisation [11]. Mg was also reported to be able to minimise the risk of osteoporosis and promote bone healing [12, 13]. Ca is one of the major elements for bone mineralisation, which is attributed to forming hydroxyapatite and calcium-phosphate [9].

Incorporating metallic ions (Sr^{+}, Fe^{3+}, Cu^{2+}, Ba^{2+}, Co^{2+}, etc.) into the akermanite structure has improved biological and mechanical performances. The addition of various metal ions into bioceramic structures has been studied, and findings showed doping can enhance bioactivity and mechanical properties of akermanite-based ceramics [4].

Phosphorus (P^{5+}) is non-metal ions that plays a crucial role in bioceramics used for bone regeneration. It is commonly incorporated in the form of phosphate ions (PO_4^{3-}). Incorporating phosphate ions into akermanite bioceramics has been explored to enhance their bioactivity. Phosphorus can promote the formation of apatite layer, support osteoblast attachment proliferation, aiding in new bone formation [14]. This modification aims to combine the favorable mechanical properties of akermanite with the biological advantages of phosphate-based ceramics.

To date, studies on phosphorus ion substitution in bioceramics—particularly akermanite—remain scarce in the literature. Therefore, this study aims to determine the effects of phosphorus-doped akermanite on the chemical/elemental, physical, and morphological properties of the akermanite-based ceramics. A range of P^{5+}-doped akermanite ceramics (1, 1.5, 2.5, and 3.5 mol%) were fabricated by wet solid-state route using high planetary ball milling. The impact of Phosphorus (P^{5+}) incorporation into host structure was then investigated through physicochemical and morphological analyses.

2. MATERIALS AND METHODS

2.1 Phosphorus-doped Akermanite Synthesis

Phosphorus-doped akermanite was produced by high-speed planetary ball milling, following the stoichiometric ratio of $Ca_2MgSi_{2-x}P_xO_7$ (where x = 1, 1.5, 2.5, and 3.5 mol%). Calcium Oxide, CaO (Sigma-Aldrich, 99.00 % pure), Magnesium Oxide (ACS reagent 97.00 %, Sigma Aldrich), Silicon Dioxide (Sigma Aldrich, 99.00 %) and Phosphorus Pentoxide, P_2O_5 (Riedel-de Haen) were weighed and placed into a zirconia jar containing zirconia ball and 48 ml of deionised water. The powders were

mixed and milled in a planetary ball mill (Fritsch P6-B) with a speed of 400 rpm for 4 h. Based on the previous study from our group, the balls-to-powder ratio and the powder-to-deionised water ratio were set at 10:1 and 1:4, respectively. Afterwards, the resultant slurry was dried for 10 hours at a temperature of 100 °C in an electric oven. The dry powders were then ground and sieved through a mesh size of 250 µm. The as-milled powders were coded as Ak for the undoped sample and 1P-Ak, 1.5P-Ak, 2.5P-Ak, and 3.5P-Ak for 1, 1.5, 2.5 and 3.5 mol% of P^{5+} -doped akermanite, respectively.

2.2 Materials Characterisation

Phase characterisation of as-milled Akermanite and P-doped Akermanite powders was performed using X-ray diffraction (XRD, Bruker D8) analysis. The as-milled powders were scanned in the range of 2θ = 10º to 90º with Cu Kα radiation (λ= 1.5406Å). Phase analysis was conducted using the PANalytical X'Pert HighScore 5 Plus software, with observational patterns matched to the International Centre for Diffraction Data (ICDD) database. Fourier transform infrared spectroscopy (FTIR) analysis was conducted in transmittance mode (%T) within a range of 400-4000 cm^{-1} to determine the functional groups in the produced powders. The mixture was prepared by combining 99 wt% of KBr with 1 wt% of the sample. The elemental analysis of as-milled powders was characterised using X-ray fluorescence (XRF, Rigaku RIX-300 wavelength dispersive). The microstructural and chemical characteristics of the produced powders were examined using a field emission scanning electron microscope/energy dispersive x-ray analysis (FESEM/EDX), Zeiss Supra™ Gemini 35 VP, equipped with an AMETEK ® microanalysis system.

3. RESULTS AND DISCUSSION

3.1 X-ray Diffraction (XRD) Analysis

Figure 1(a) shows the X-ray Diffraction (XRD) pattern of a range of P-doped as-milled powders produced using high-energy planetary mill. Some transient compounds, such as Wollastonite (ICDD #01-090-4960), and Clinoenstatite (ICDD #00-035-0610), were formed. There were also unreacted raw materials such as quartz (ICDD #01-070-3755), periclase (ICDD #00-043-1022), and lime (ICDD #04-016-3215). This XRD result shows single phase akermanite could not be formed by subjecting the powders only to intense mechanical activation at ambient temperature. Therefore, further heat treatment at high temperature is further required [15]. A similar observation was previously reported in the literature [7, 15]. This has motivated the researchers to investigate the phase formation of $Ca_2MgSi_2O_7$ [7, 15]. For instance, Myat et al. [15] reported that below 700 °C, transient phases like clinoenstatite, wollastonite, and monticellite were detected due to incomplete solid-state reactions and insufficient atomic diffusion. A single phase of akermanite could only be achieved at a temperature 1000 °C; at this temperature, the thermal energy is sufficient to overcome activation energy barriers, allowing for the complete diffusion and rearrangement of Ca^{2+}, Mg^{2+} and SiO_4^{4-} ions. Additionally, at lower temperatures, reaction kinetics are sluggish, and intermediate phases remain stable due to their lower activation energies. The complete transformation into akermanite at 1000 °C occurs because this temperature provides the necessary Gibs free energy reduction, enabling the crystallisation of a thermodynamically stable $Ca_2MgSi_2O_7$ phase while eliminating metastable phases [15].

Figure 1(b) shows the highest peaks intensity of akermanite and P-doped akermanite as-milled powders between 26.5º and 27º, which shows that the doping of P^{5+} resulted in a minor displacement of the diffraction peaks to the higher angles with increasing P^{5+} concentration. The peak shifts are attributed as an indicator of successful doping and the extent of lattice changes due to interstitial doping of P^{5+} at the Si^{4+} site of the host structure. Using the cation's charge balance and effective ionic radii (r) in relation to the coordination number (CN), the P^{5+} ion, which has a smaller ionic radius (r = 0.17Å) than Si^{4+} (r = 0.26Å), causes the surrounding atom to move closer together [16]. According to the Goldschmidt's rules, partial ionic substitution is feasible when the difference in ionic radii between the substituting ions less than 15 %. In this case, the ionic radii of P^{5+} and Si^{4+} differ by approximately 5 %,

suggesting that P^{5+} ions can reasonably be accommodated at the Si^{4+} sites within the akermanite structure [17].

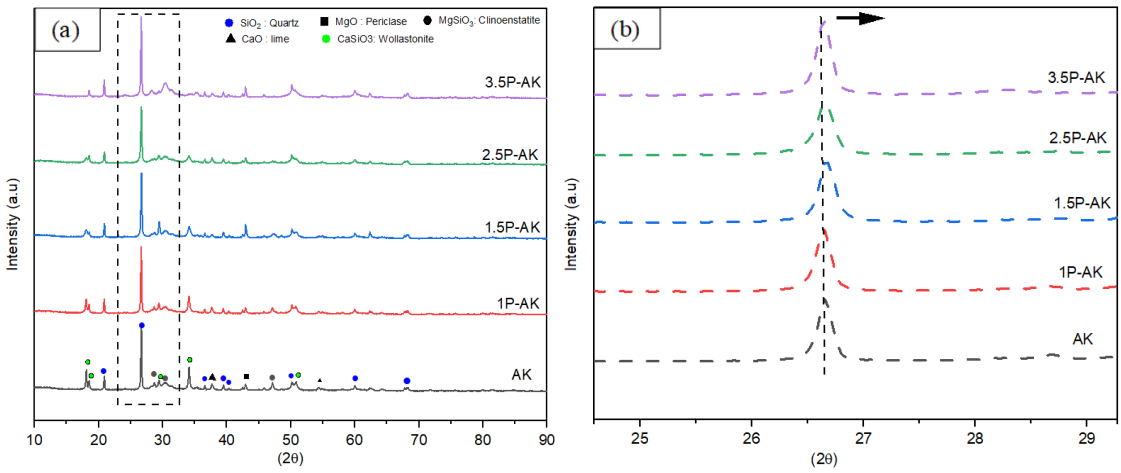

Figure 1: (a) XRD patterns of P-doped akermanite-based as-milled powders produced using high-energy planetary mill in the range of 2θ = 10º-90º (Ak, 1P-Ak, 1.5P-Ak, 2.5P-Ak, 3.5P-Ak) and (b) partial peak shifts in the range of 2θ = 26.5º-27º

3.2 FTIR Analysis

Figure 2 shows the FTIR of the as-milled powders (at varying P^{5+} concentrations). The spectra exhibited characteristic peaks corresponding to functional groups such as Si-O-Si, O-Mg-O, and O-Ca-O, which are typically observed in material containing silicon, magnesium, and calcium-key components of the raw materials used in the preparation of akermanite powders [7, 18].

Table 1 presents the detailed wavenumber position of these functional groups for each sample, providing clearer insight into the spectral shifts induced by phosphate doping. The bending modes for the v(O-Ca-O) functional group was identified at 419 cm^{-1} for Ak, and showed slight shift to lower wavenumber with increasing P^{5+} content, at 416.94 cm^{-1}, 417 cm^{-1}, 402.32 cm^{-1}, 402.00 cm^{-1} for 1P-Ak, 1.5P-Ak, 2.5P-Ak, and 3.5P-Ak, respectively. Similarly, the v(O-Mg-O) bending mode appeared at 466.18 cm^{-1} in Ak and gradually decreased to 457.99 cm^{-1} in 3.5P-Ak. These slight shifts suggest minor structural adjustments due to phosphate incorporation. The bending band corresponding to Ca=O was found at 874.69 cm^{-1} in Ak and showed minimal variation, ranging between 874.21 and 875.43 cm^{-1} in the doped samples. The absorption bands were associated with the double peaks of v(O-Si-O) at 779.86 cm^{-1} and 799.15 cm^{-1} in Ak [18]. These bands remained stable across the doped samples, with the lower wavenumber peaks ranging from 779.35 to 780.16 cm^{-1} and the higher from 798.92 to 799.69 cm^{-1}. Furthermore, the symmetric stretching identified at 1091.16 cm^{-1} was associated with the functional group of Si-O-Si in Ak, also showed slight decreased with increasing dopant levels at 1090.84, 1087.82, 1090.04, 1089.74 cm^{-1}, for 1P-Ak, 1.5P-Ak, 2.5P-Ak, and 3.5P-Ak, respectively [1, 4, 7, 15, 18].

The substitution of P^{5+} into the akermanite structure did not significantly affect the functional groups, likely due to the low concentration of the dopant. Consequently, the FTIR spectra of the P-doped akermanite closely resembled those of the undoped as-milled powders, suggesting that the structure remained stable at the given dopant level [15].

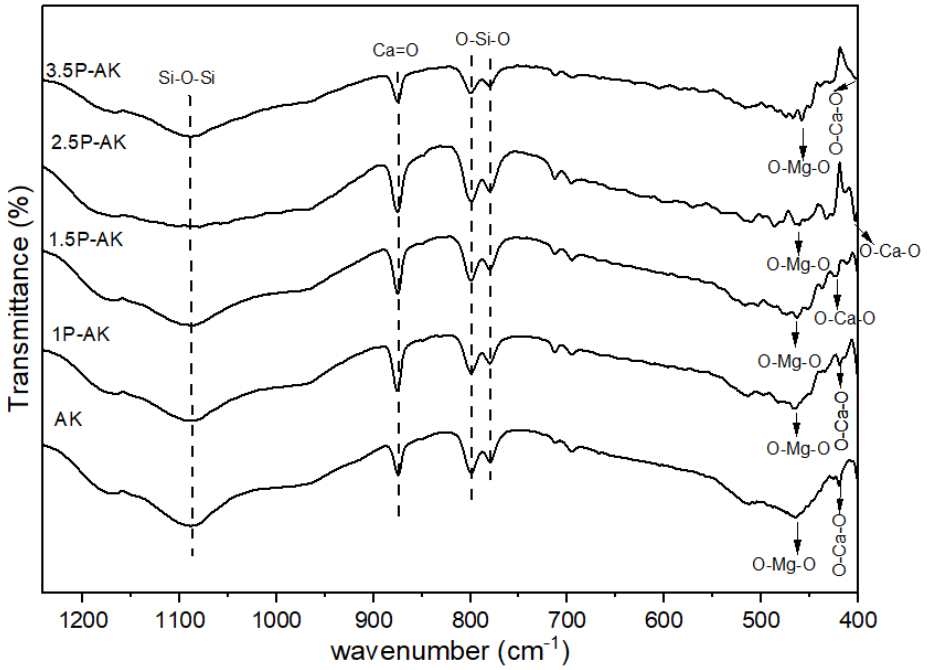

Figure 2: The FTIR spectra of P-doped akermanite-based as-milled powders produced using high-energy planetary mill (Ak, 1P-Ak, 1.5P-Ak, 2.5P-Ak, 3.5P-Ak)

Table 1: The wavelength of FTIR spectra of AK and P-doped AK

Functional group	Characteristic	Wavelength (cm^{-1})				
		Ak	1P-Ak	1.5P-Ak	2.5P-Ak	3.5P-Ak
v(O-Ca-O)	Bending modes	419.00	416.94	417.00	402.32	402.00
v(O-Mg-O)	Bending modes	466.18	465.91	466.52	462.26	457.99
v(O-Si-O)	Absorption band	779.86, 799.15	779.88, 798.99	779.93, 798.92	780.16, 799.22	780.37, 799.69
v(Ca=O)	Bending band	874.69	874.61	874.29	875.49	875.33
v(Si-O-Si)	Symmetric stretching	1091.16	1090.84	1087.82	1090.04	1089.74

3.3 X-ray Fluorescence (XRF) Analysis

Table 2 presents the elemental composition of as-milled powders for the P-Ak sample, analysed using X-ray fluorescence (XRF). The results confirm the presence of key akermanite elements-Ca, Mg, Si and O-along with trace amount of phosphorus (P). The detected phosphorus levels show an increasing trend corresponding to the mol% P added. Additionally, trace amount of zirconium (Zr) were observed in all as-milled powders [19]. This contamination arises during high-energy milling, where friction between the zirconia milling media and the vial causes chipping of the zirconia balls, leading to Zr incorporation into the powders [15, 19]. The detected Zr content in the as-milled powders is minimal (typically below 1 wt%, as reported in similar studies) and falls in within acceptable limits for biomaterials [20, 21]. Zirconia (ZrO_2) is widely used in biomedical applications due to its excellent biocompatibility, corrosion resistance, and mechanical strength. Studies have shown that Zr level below 2 wt% do not cause cytotoxicity and are considered safe for biomedical use [20, 21]. Additionally, ZrO_2 is bioinert and does not induce adverse reactions in physiological environments, making it a common component in orthopeadic and dental implants [22].

Based on the elemental analysis, 3.5P-Ak was identified as the optimal composition, as it contained the highest level of dopant incorporated into the akermanite host structure. However, confirming the initial assumption that P^{5+} substitutes Si^{4+} is not feasible at this stage. Heat treatment is necessary to ensure proper bonding configuration and complete the reaction in forming single phase akermanite ceramics.

Table 2: XRF elemental analysis of as-milled powders with various P concentrations

Elemental (mass%)	Sample				
	Ak	**1P-Ak**	**1.5P-Ak**	**2.5P-Ak**	**3.5P-Ak**
Ca	47.54	39.14	38.71	39.81	38.73
Mg	4.47	8.46	8.24	7.31	8.57
Si	11.13	13.37	13.85	13.77	13.24
P	-	0.16	0.27	0.41	0.60
O	35.17	37.20	37.48	37.36	37.44
Zr	1.68	1.65	1.45	1.34	1.42

3.4 Morphology Analysis

Figures 3(a) to (e) presents the micrographs of powders milled at 400 rpm for 4 h. All sample displayed similar morphologies, characterized by agglomerated particles with irregular shapes, likely can attributed to van der Walls attraction forces between particles [15]. Despite the difference in composition, the introduction of the dopant did not result in any noticeable morphological changes in the akermanite structure. no significant changes occurred when the dopant was introduced into the akermanite structure. Further analysis Transmission Electron Microscopy (TEM) is planned for future studies to obtain more comprehensive assessment of the particle morphology and size.

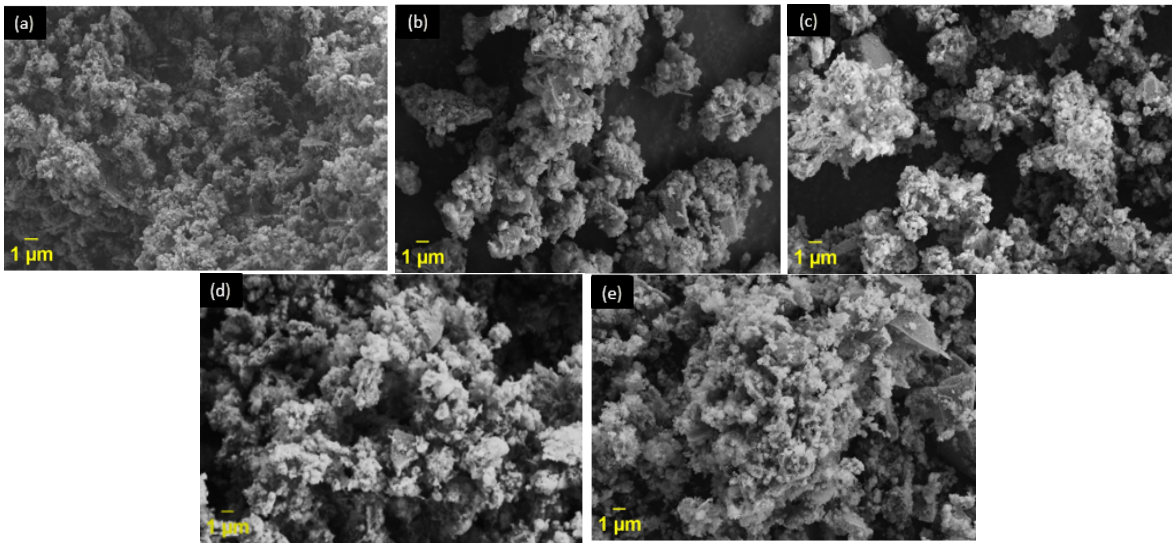

Figure 3: Surface morphology of as-milled powders: (a) AK, (b) 1P-AK, (c) 1.5P-AK, (d) 2.5P-AK and (e) 3.5P-AK (Scale bar = 1 µm and Magnification = 10.000 X

The elemental analysis of the akermanite and P-doped akermanite-based as-milled powders was identified using Energy dispersive X-ray analysis (EDX). Table 3 demonstrated that Ca, Mg, Si, and O are the primary constituents of the powders, whereas P is the trace element. This indicates that P^{5+} has partially substituted into the host structure.

Table 3: EDX elemental analysis of as-milled powders

Elemental (wt%)	Sample				
	AK	1P-AK	1.5P-AK	2.5P-AK	3.5P-AK
Ca	12.94	8.56	10.47	10.13	8.68
O	53.84	20.14	41.95	45.61	40.58
Mg	11.29	11.36	9.16	11.81	13.79
Si	21.93	38.83	28.15	21.94	24.01
P	-	21.12	10.28	10.52	12.94
P/Si	-	0.54	0.37	0.48	0.54

4. CONCLUSIONS

Phosphorus-doped akermanite as-milled powders (1, 1.5, 2.5 and 3.5 mol%) have been successfully synthesised using high-energy planetary ball milling at 400rpm for 4 h. At this stage, a single-phase akermanite was not achieved, as evidenced by the presence of multiple phases such as wollastonite, clinoenstatite, quartz, periclase and lime. The incorporation of P^{5+} into the akermanite structure increased proportionally with the amount of P^{5+} added. A subsequent heat treatment at 1100 ℃ is necessary to promote the formation of single-phase akermanite and ensure complete reactions. Regardless of compositions, all synthesised powders exhibited agglomerated particles with irregular morphology. Among the tested formulation, 3.5 mol% P^{5+} was identified as the optimal, containing the highest phosphorus content (12.94 wt%), which is closest to that of native bone (~17 wt%). Phosphorus-doped akermanite holds significant potential for biomedical application, particularly in scaffold fabrication for bone regeneration, due to its enhanced bioactivity and tunable mechanical properties.

Acknowledgements

The funding for this research was provided by the Ministry of Higher Education Malaysia under the Fundamental Research Grant Scheme (FRGS) Grant no. FRGS/1/2021/ TK0/USM/03/4.

Author Contributions

All authors participated in manuscript drafting, data analysis, critical revision, and collectively accepted responsibility for every aspect of work.

Disclosure of Conflict of Interest

The authors have no disclosures to declare.

Compliance with Ethical Standards

The work is compliant with ethical standards.

References

[1] Mohammadi, H., Baba I. Y. M., Shariff, K. A. & Mohd, N. A. F. (2021). Microstructure evolution, grain growth kinetics and mechanical properties of $Ca_2MgSi_2O_7$ bioceramics sintered at various temperatures. *Processing and Application of Ceramics*, 15(4), 357-365.

[2] Ahmadipour, M., Mohammadi, H., Pang, A. L., Arjmand, M., Ayode Otitoju, T., U. Okoye, P. & Rajitha, B. (2022). A review: silicate ceramic-polymer composite scaffold for bone tissue engineering. *International Journal of Polymeric Materials and Polymeric Biomaterials*, 71(3), 180-195.

[3] Alecu, A. E., Costea, C. C., Surdu, V. A., Voicu, G., Jinga, S. I. & Busuioc, C. (2022). Processing of calcium magnesium silicates by the sol–gel route. *Gels*, 8(9), 574.

[4] Myat-Htun, M., Ahmad-Fauzi, M. N., Kawashita, M., Yanny Marliana, B. I. (2021). Tailoring mechanical and in vitro biological properties of calcium–silicate based bioceramic through iron doping in developing future material. *Journal of the Mechanical Behavior of Biomedical Materials*, 128, 105122.

[5] Parauha, Y. R., Sahu, V. & Dhoble, S. J. (2021). Prospective of combustion method for preparation of nanomaterials: A challenge. *Materials Science and Engineering: B*, 267, 115054.

[6] Mahtabian, S., Yahay, Z., Mirhadi, S. M. & Tavangarian, F. (2020). Synthesis and characterization of hierarchical mesoporous‐macroporous TiO_2-ZrO_2 nanocomposite scaffolds for cancellous bone tissue engineering applications. *Journal of Nanomaterials*, 2020(1), 8305871.

[7] Tavangarian, F., Zolko, C. A. & Davami, K. (2021). Synthesis, characterization and formation mechanisms of nanocrystalline akermanite powder. *Journal of Materials Research and Technology*, 11, 792-800.

[8] Zadehnajar, P., Mirmusavi, M. H., Soleymani Eil Bakhtiari, S., Bakhsheshi-Rad, H. R., Karbasi, S., RamaKrishna, S., & Berto, F. (2021). Recent advances on akermanite calcium-silicate ceramic for biomedical applications. *International Journal of Applied Ceramic Technology*, 18(6), 1901-1920.

[9] Hayann, L., Ciancaglini, P., Ramos, A.P. & Napierala, D. (2024). Calcium and phosphate and their role in matrix vesicles: A biological view. In *Mineralizing Vesicles*, (Academic Press), pp. 151-173.

[10] Lan, H., Zhang, M., Chen, X., Huang, Z. & Yin, G. (2020). Designing a novel CaO–MgO–SiO_2-based multiphase bioceramic with adjustable ion dissolution behavior for enhancing osteogenesis. *Smart Materials in Medicine*. (3), 94–103.

[11] Ciosek, Ż., Kot, K., Kosik-Bogacka, D., Łanocha-Arendarczyk, N., & Rotter, I. (2021). The effects of calcium, magnesium, phosphorus, fluoride, and lead on bone tissue. *Biomolecules*, 11(4), 506.

[12] Golzar, H., Mohammadrezaei, D., Yadegari, A., Rasoulianboroujeni, M., Hashemi, M., Omidi, M., Yazdian, F., Shalbaf, M. & Tayebi, L. (2020). Incorporation of functionalized reduced graphene oxide/magnesium nanohybrid to enhance the osteoinductivity capability of 3D printed calcium phosphate-based scaffolds. *Composites Part B: Engineering*, 185, 107749.

[13] Ghițulică, C. D., Cucuruz, A., Voicu, G., Cucuruz, A. T., Dinescu, S., Selaru, A. & Costache, M. (2020). Ceramics based on calcium phosphates substituted with magnesium ions for bone regeneration. *International Journal of Applied Ceramic Technology*, 17(1), 342-353.

[14] Du, T., Niu, Y., Jia, Z., Liu, Y., Qiao, A., Yang, H. & Niu, X. (2022). Orthophosphate and alkaline phosphatase induced the formation of apatite with different multilayered structures and mineralization balance. *Nanoscale*. 14(5), 1814-1825.

[15] Myat-Htun, M., Mohammadi, H., Mohd N. A. F., Kawashita, M. & Baba I. Y. M.(2021). Comprehensive investigation of phase formation mechanism and physico-mechanical properties of Ca-Mg-Silicate. *ASEAN Engineering Journal*, 11(2), 37-50.

[16] Misra, K. C. (2012). *Introduction to geochemistry: principles and applications*. 1st edition (John Wiley & Sons), pp. 24-28.

[17] Soykan, C. (2020). A theoretical approach to the structural, elastic and electronic properties of $Ti_{8-x}V_{4-y}Mo_{x+y+z}Al_{4-z}$ lightweight shape memory alloys for biomaterial implant applications. *Physica B: Condensed Matter*, 598, 412416.

[18] Mohd Rosli, N. L. & Baba Ismail, Y. M. (2024). Zero-value dental mould waste: an innovative pathway for high purity calcium source enabling the production of akermanite ceramics. *Journal of the Australian Ceramic Society*, 60(5), 1381-1392.

[19] Shakrani, S. A., Ayob, A., Rahim, M. A. & Alias, S. (2020). Properties of pulverized kaolin particles via ball-to-powder weight ratios milling process: XRF and Zetasizer particle size analysis. In *IOP Conference Series: Earth and Environmental Science,* 476, 012070.

[20] Sivasankar, M. V., Chinta, M. L. & Rao, P. S. (2024). Zirconia based composite scaffolds and their application in bone tissue engineering. *International Journal of Biological Macromolecules*, 265(1), 130558.

[21] Parameswaranpillai, J., Ganguly, S., Das, P. & Gopi, J. A. (2024*). Fiber and Ceramic Filler-Based Polymer Composites for Biomedical Engineering*, (Springer), pp. 289-313.

[22] Basheer, Al-Naib. Uday M. (2023). *Zirconia - New Advances, Structure, Fabrication and Applications*. 1st edition (IntechOpen), pp. 7-24.